Supplementary Information (SI) for Green Chemistry.
This journal is © The Royal Society of Chemistry 2025

Supporting Information for

Unlocking the Activity of Lattice Oxygen in P-Engineered MoO_2 for Efficient Oxygen Evolution Reaction: A d-Band Center Modulation Perspective

Yi Xu,[a] Fanshu Yuan,*[a, b] Xiaotian Xie,[a, b] Jinhui Tong,[c] Cheng Min,[a, b] Qian Zhang,[a, b] Jie Tang,[a, b] Jie Liu,[a, b] Tingting Lv[a, b] and Qianli Zhang*[a, b]

a. School of the Chemistry and Life Sciences, Suzhou University of Science and Technology, Suzhou 215009, China.
b. Key Laboratory of Advanced Electrode Materials for Novel Solar Cells for Petroleum and Chemical Industry of China, Suzhou University of Science and Technology, Suzhou 215009, China.
c. School of Chemistry and Chemical Engineering, Northwest Normal University, Lanzhou, 730000, China.

Experimental section

In-situ ^{18}O Isotope Labeling Coupled with DEMS measurements

The in-situ DEMS measurements were conducted using a mass spectrometer with heavy oxygen water ($H_2{}^{18}O$) to explore the involvement of lattice oxygen during the OER process. The catalyst was first subjected to ^{18}O isotope labeling by cyclic voltammetry in a 1 M KOH electrolyte prepared with $H_2{}^{18}O$ within a potential range of 1.1-1.7 V (vs. RHE) for 10 cycles at a scan rate of 5 mV s^{-1}. This was followed by chronoamperometry at 1.7 V for 10 min to enrich the catalyst surface with ^{18}O species, during which the mass signals of the evolved gaseous products at m/z=32 ($^{16}O_2$), 34 ($^{16}O^{18}O$), and 36 ($^{18}O_2$) were continuously monitored. Subsequently, the isotope-labeled catalyst was transferred to a 1 M KOH electrolyte prepared with $H_2{}^{16}O$ and evaluated for the oxygen evolution reaction (OER) by CV in the potential range of 1.1-1.6 V at a scan rate of 5 mV s^{-1}. Prior to all electrochemical measurements, the electrolytes were purged with high-purity N_2 to remove dissolved oxygen.

Fig. S1

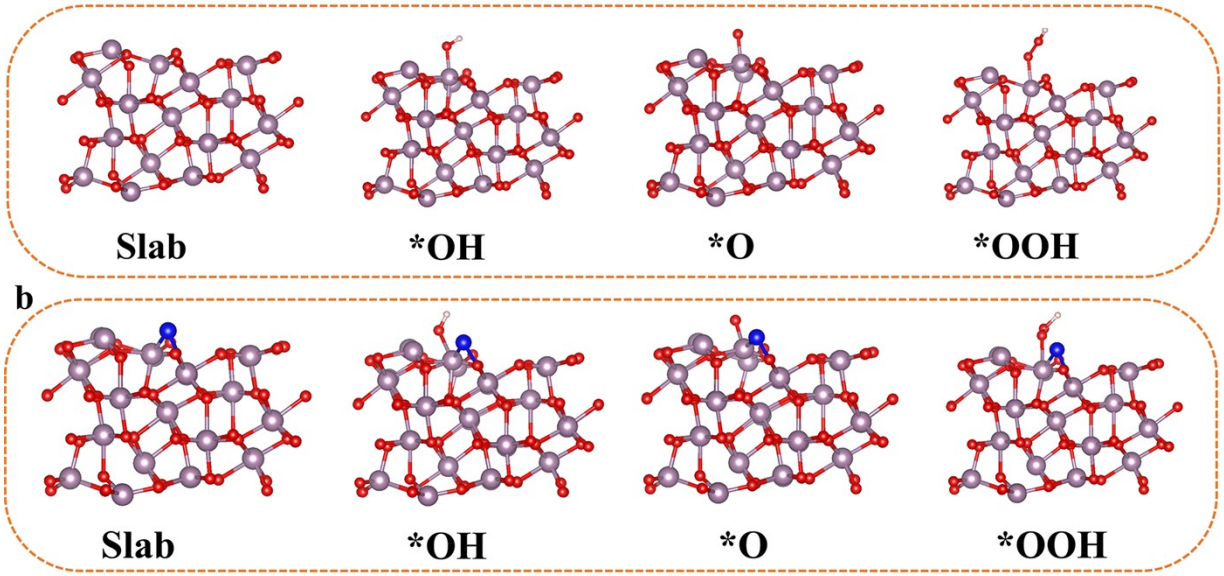

Fig. S1 Structural evolution of the OER process of (a) MoO_2 and (b) P-MoO_2 following the AEM.

Fig. S2

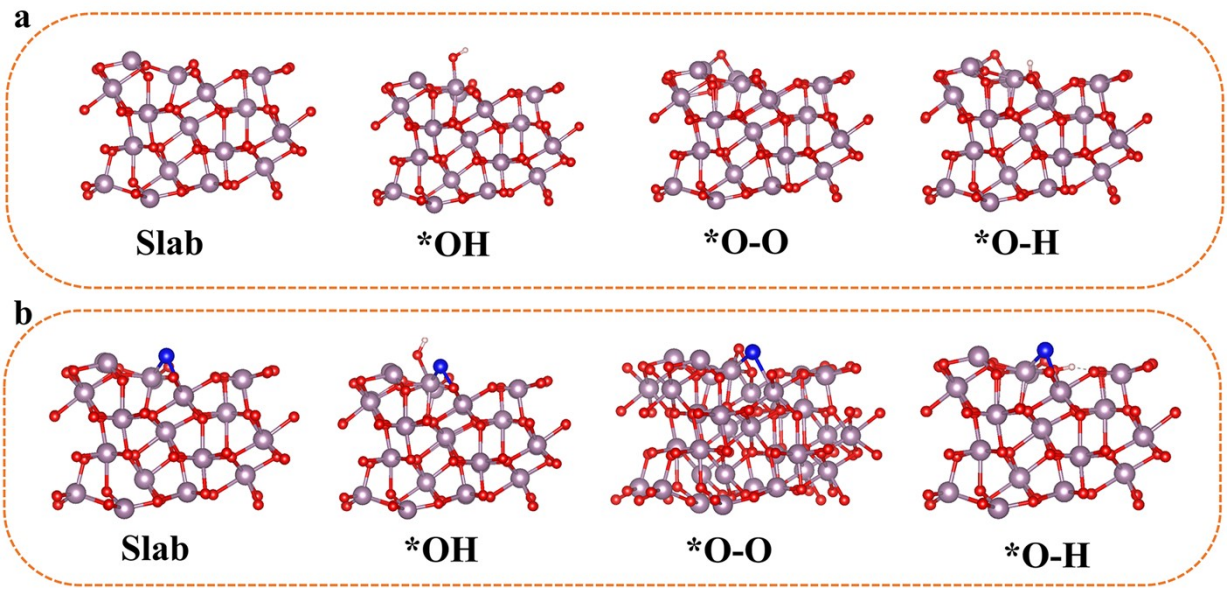

Fig. S2 Structural evolution of the OER process of (a) MoO_2 and (b) P-MoO_2 following the LOM.

Fig. S3

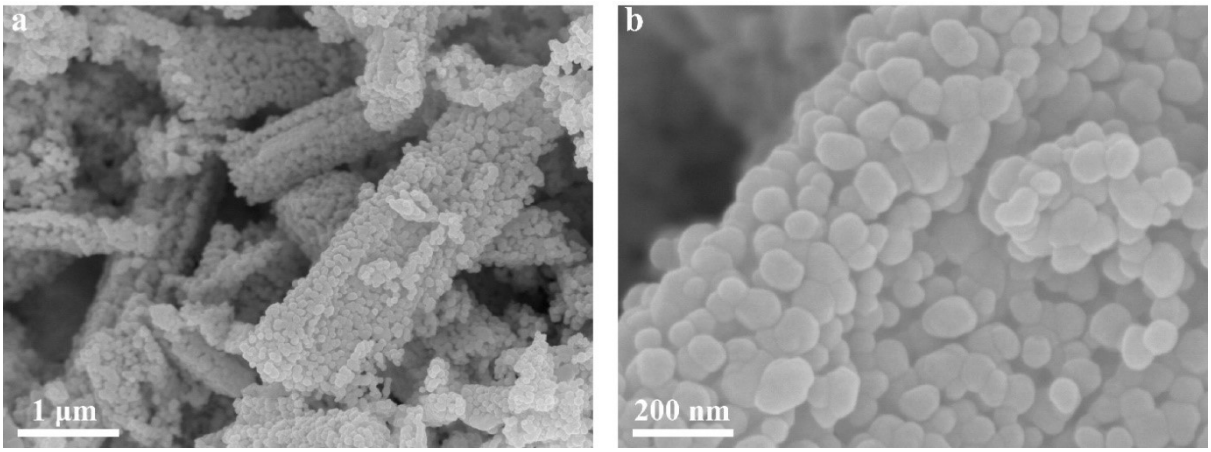

Fig. S3 SEM image of MoO_2-800.

Fig. S4

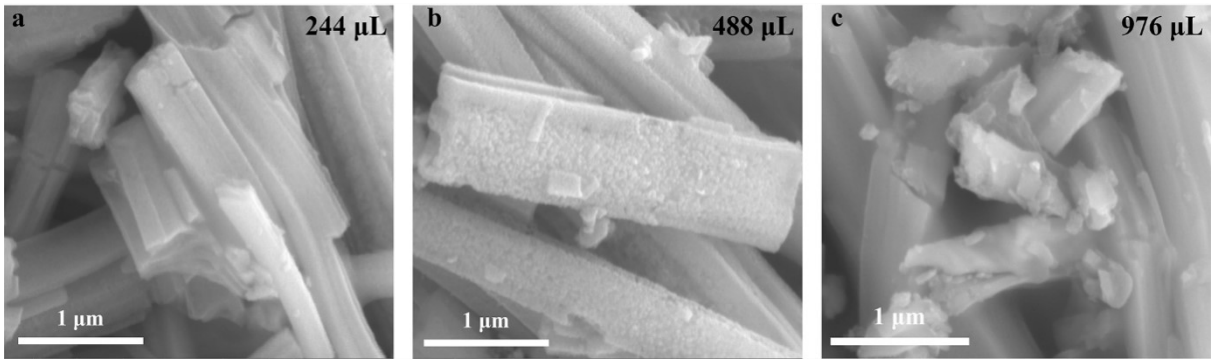

Fig. S4 SEM images of P-MoO_2-800 prepared with different volume of PA at 800 °C. (a) 244 µL, (b) 488 µL, (c) 976 µL.

Fig. S5

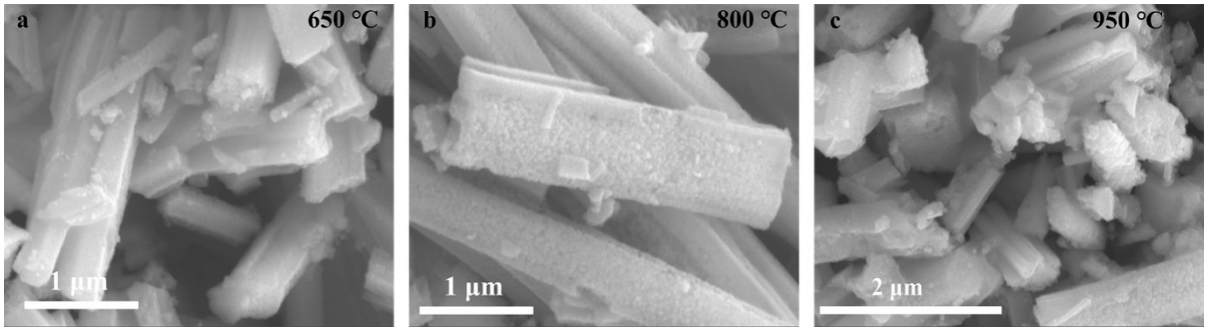

Fig. S5 SEM images of P-MoO_2-X prepared at different phosphating temperatures. (a) 650 ℃, (b) 800 ℃, (c) 950 ℃.

Fig. S6

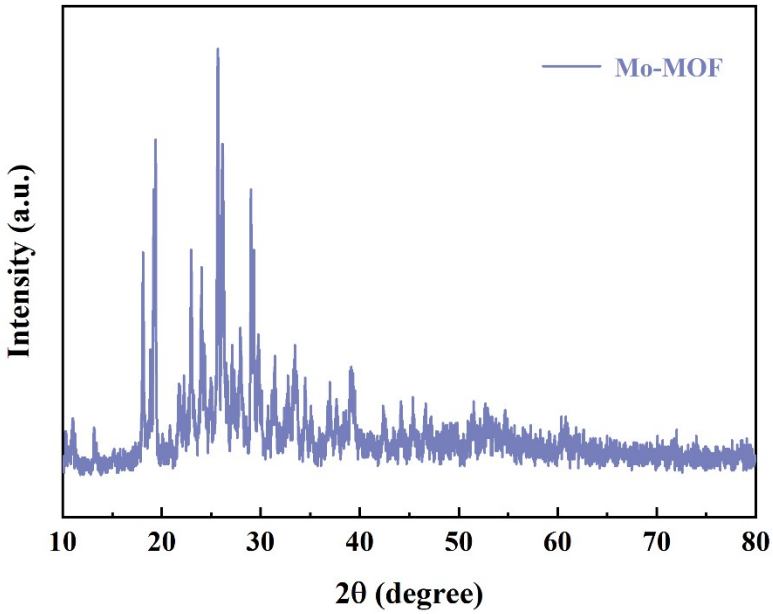

Fig. S6 XRD patterns of the Mo-MOF.

Fig. S7

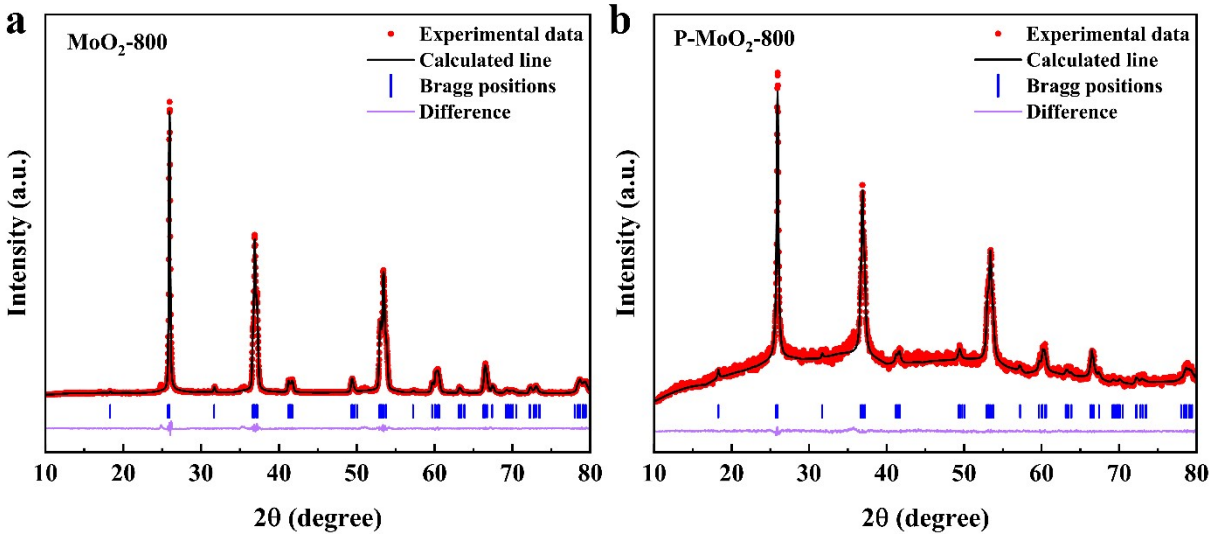

Fig. S7 XRD refined patterns of the (a) MoO_2-800 and (b) P-MoO_2-800.

Fig. S8

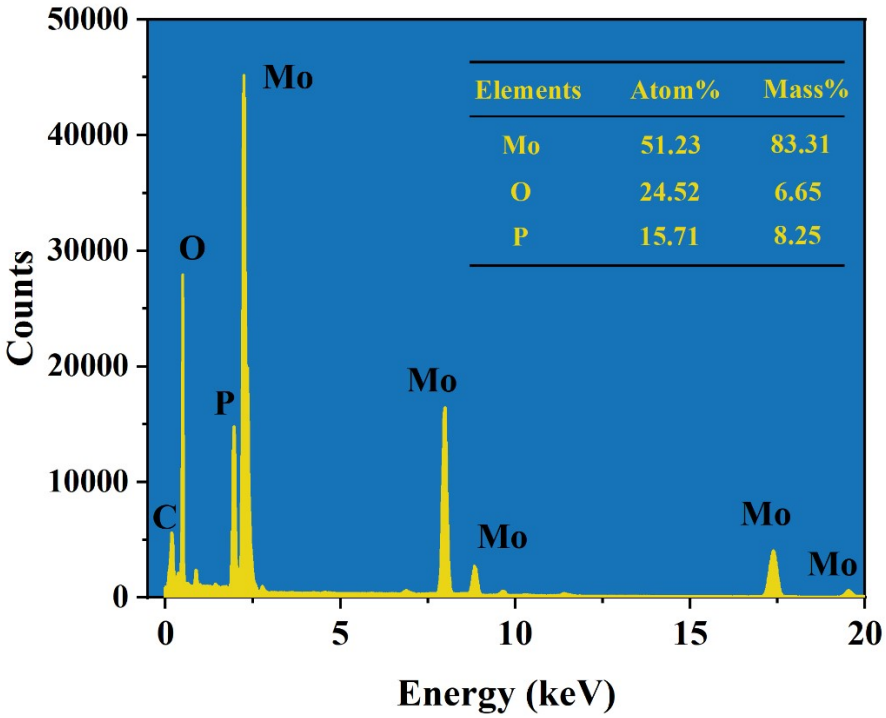

Fig. S8 EDS spectrum of P-MoO_2-800.

Fig. S9

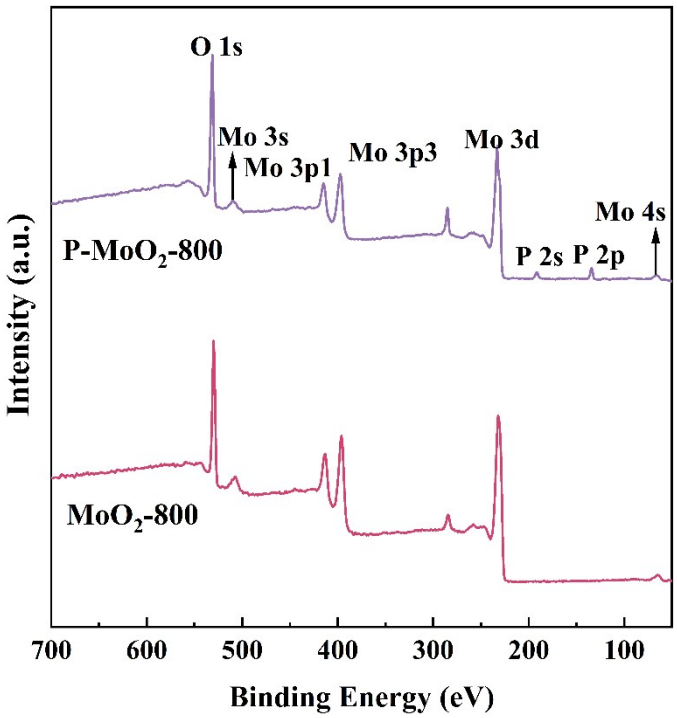

Fig. S9 XPS full spectra of MoO_2-800 and P-MoO_2-800.

Fig. S10

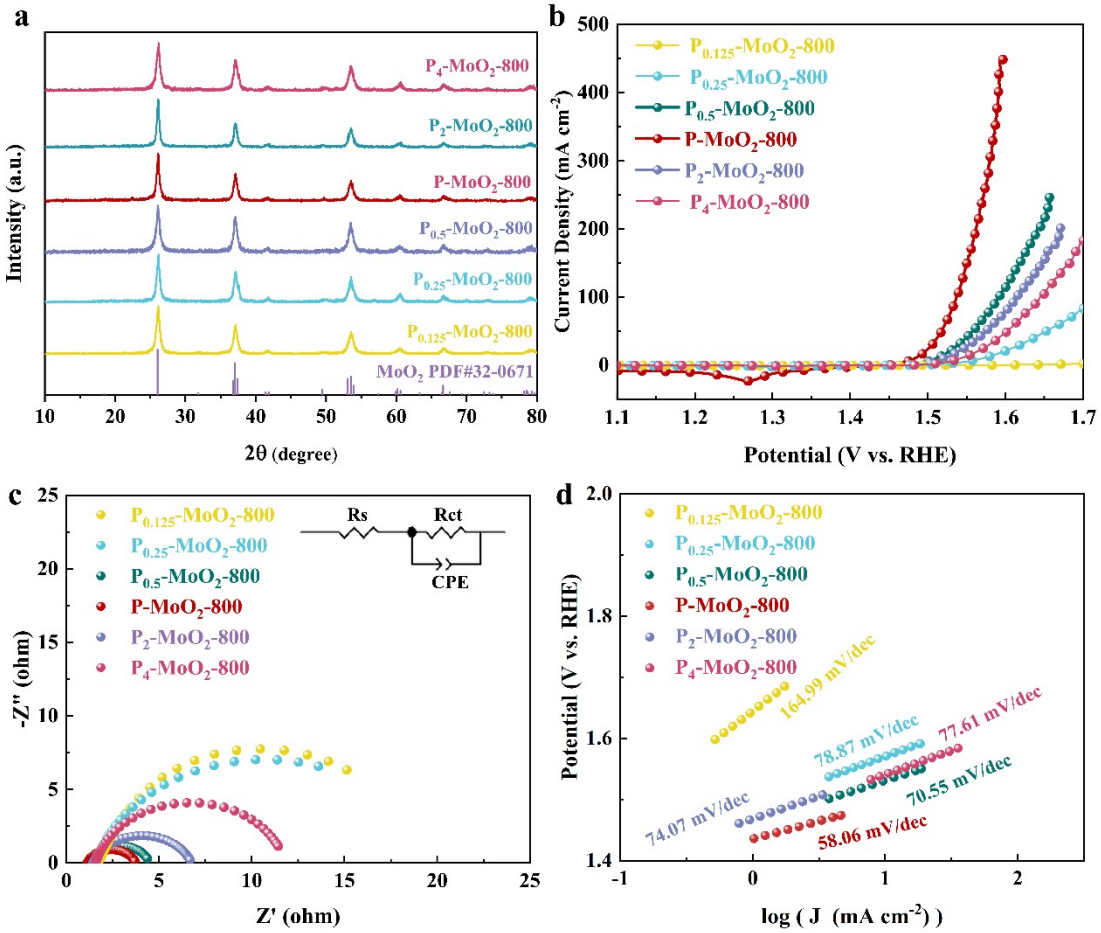

Fig. S10 (a) XRD patterns, (b) LSV curves, (c) Nyquist plots collected at 1.51 V vs. RHE, (d) Tafel slope of P-MoO_2-800 prepared with different volumes of PA.

Fig. S11

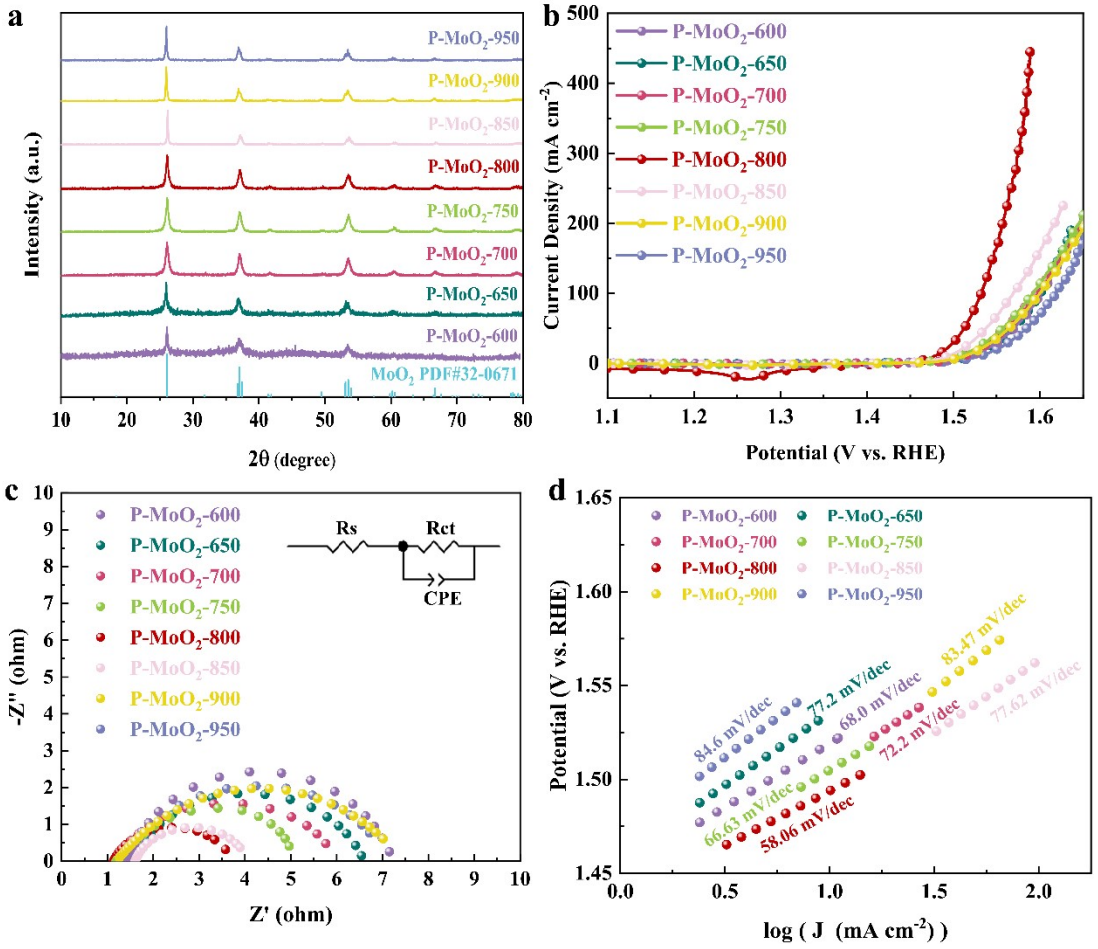

Fig. S11 (a) XRD patterns (b) LSV curves, (c) Nyquist plots collected at 1.51 V vs. RHE, (d) Tafel slope of P-MoO_2 prepared at different pyrolysis temperatures.

Fig. S12

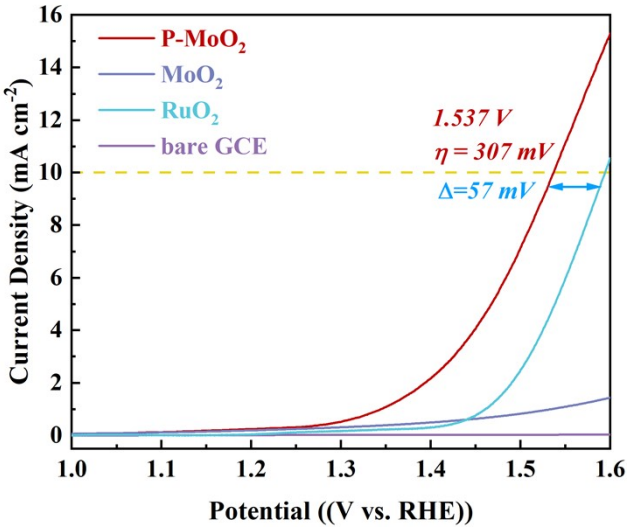

Fig. S12 LSV curves of P-MoO_2, MoO_2, and RuO_2 catalysts loaded on glassy carbon electrodes measured in 1.0 M KOH solution.

Fig. S13

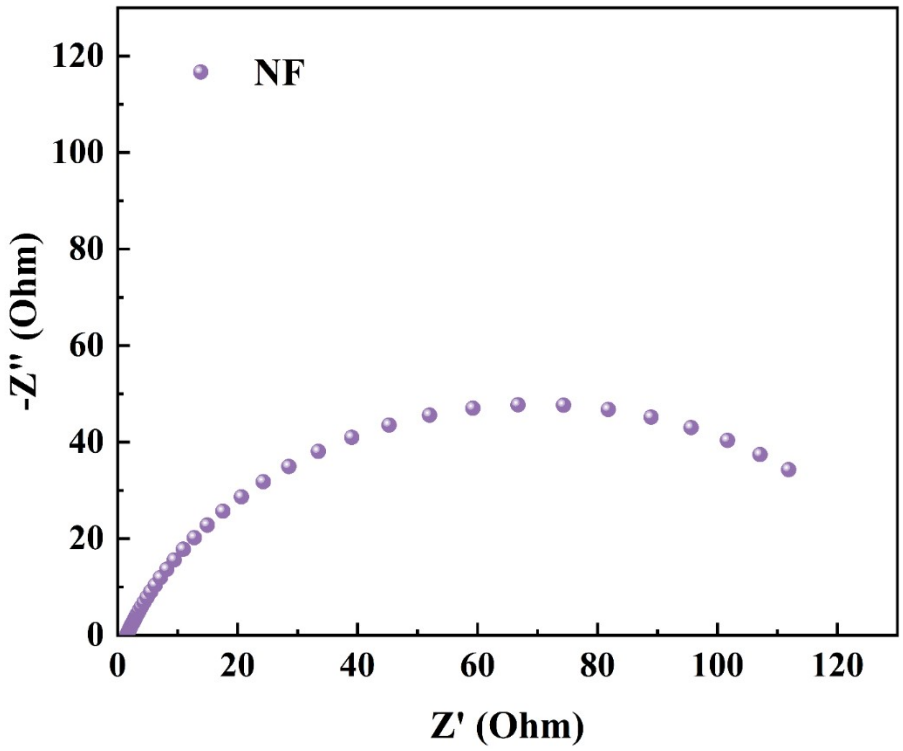

Fig. S13 Nyquist plots of bare NF recorded at 1.51 V vs. RHE.

Fig. S14

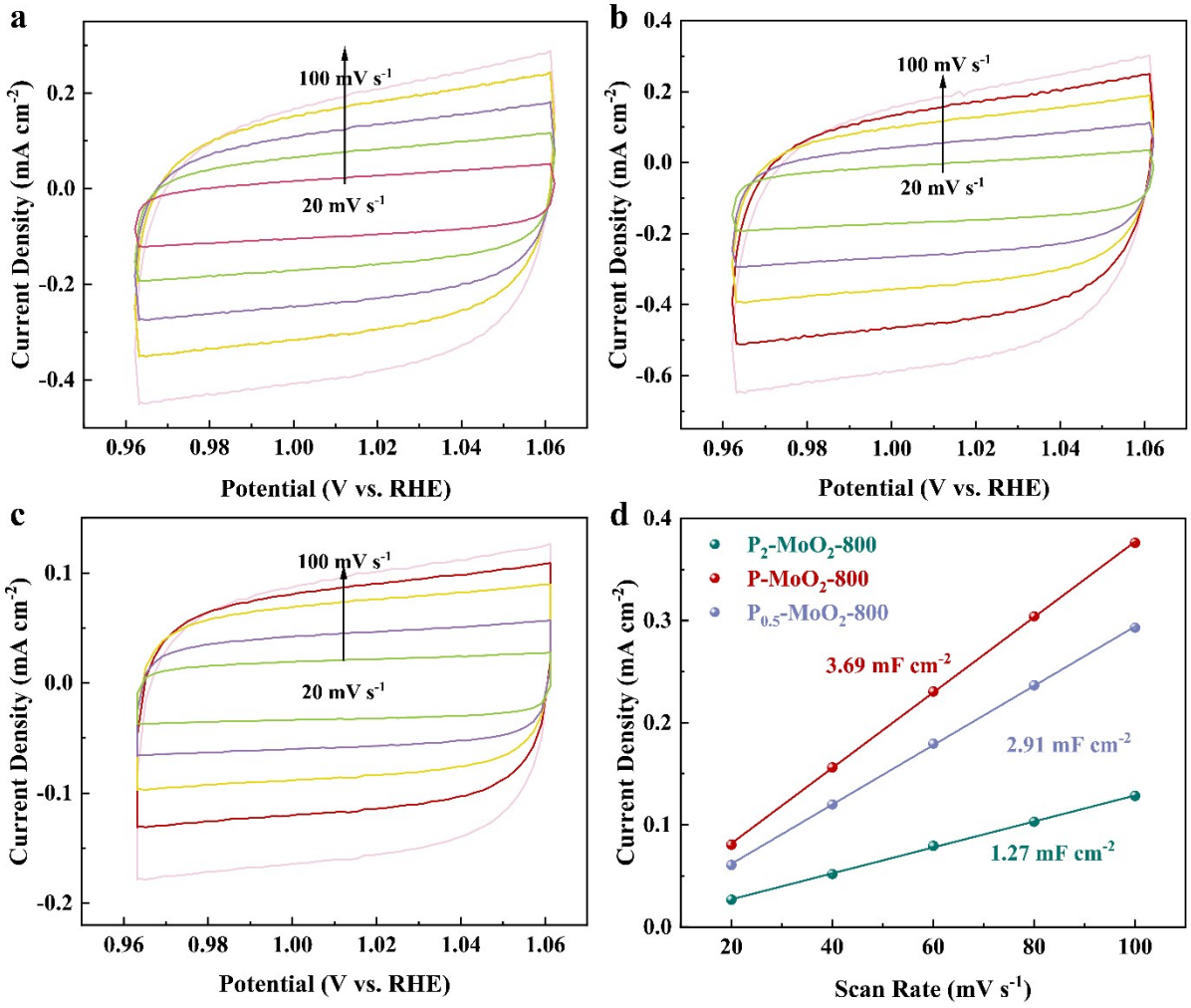

Fig. S14 Typical CV curves of (a) $P_{0.5}$-MoO_2-800, (b) P-MoO_2-800, (c) P_2-MoO_2-800 in a non-faradaic region in 1.0 M KOH for OER at the scan rates from 20 mV s^{-1} to 100 mV s^{-1}, (d) The fitted C_{dl} at the non-faradaic potential range.

Fig. S15

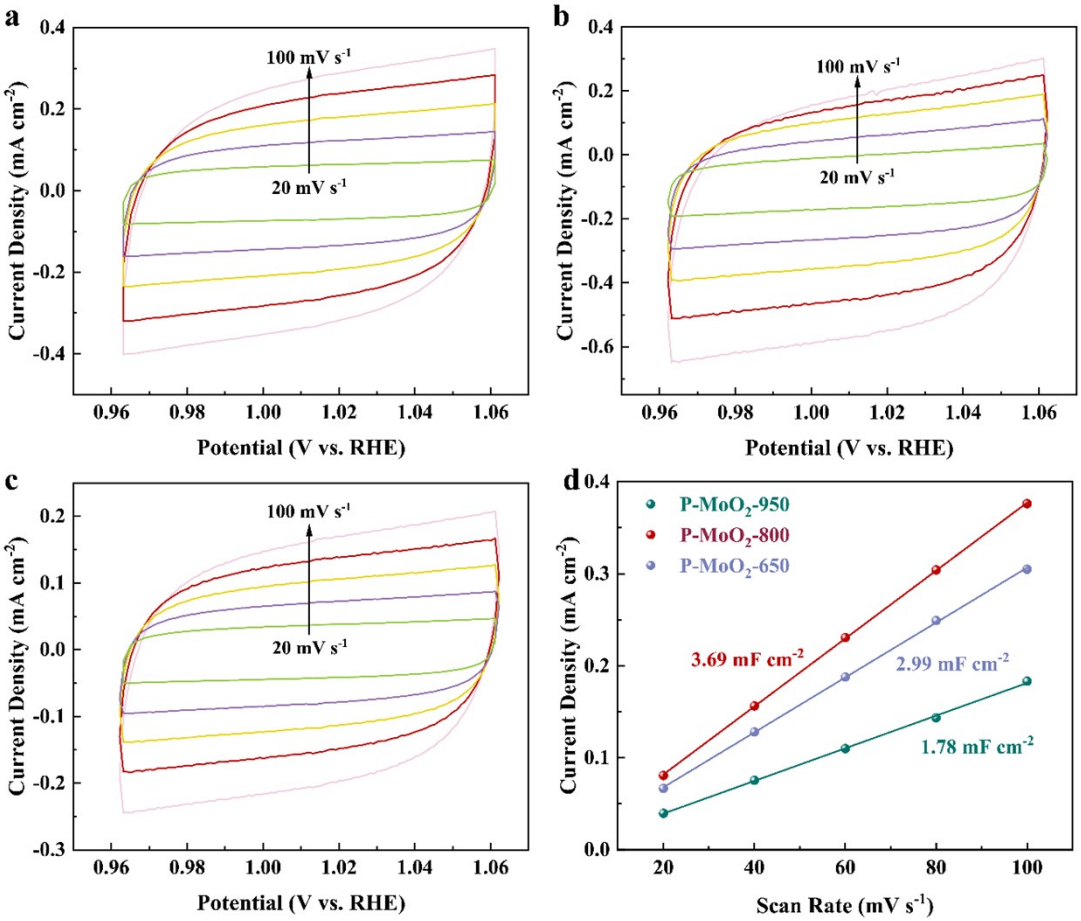

Fig. S15 Typical CV curves of (a) P-MoO_2-650, (b) P-MoO_2-800, (c) P-MoO_2-950 in a non-faradaic region in 1.0 M KOH for OER at the scan rates from 20 mV s^{-1} to 100 mV s^{-1}, (d) The fitted C_{dl} at the non-faradaic potential range.

Fig. S16

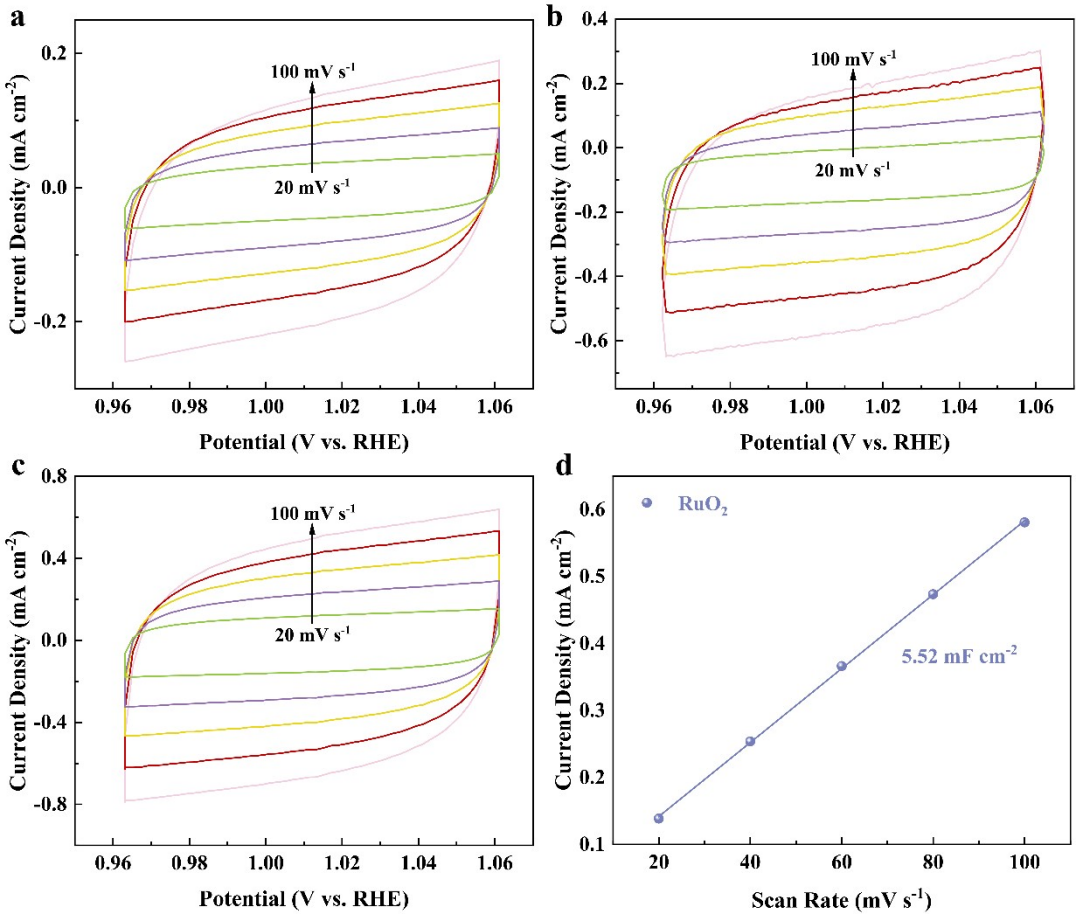

Fig. S16 Typical CV curves of (a) MoO_2, (b) P-MoO_2-800, (c)RuO_2 in a non-faradaic region in 1.0 M KOH for OER at the scan rates from 20 mV s^{-1} to 100 mV s^{-1}, (d) The fitted C_{dl} of RuO_2 at the non-faradaic potential range.

Fig. S17

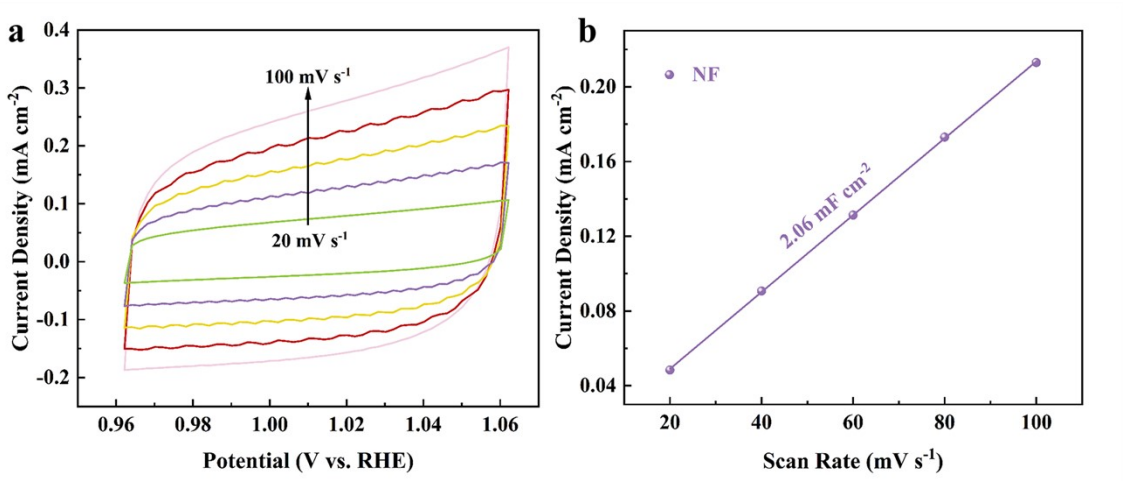

Fig. S17 Typical CV curves of NF in a non-faradaic region in 1.0 M KOH for OER at the scan rates from 20 mV s^{-1} to 100 mV s^{-1}, (b) The fitted C_{dl} of NF at the non-faradaic potential range.

Fig. S18

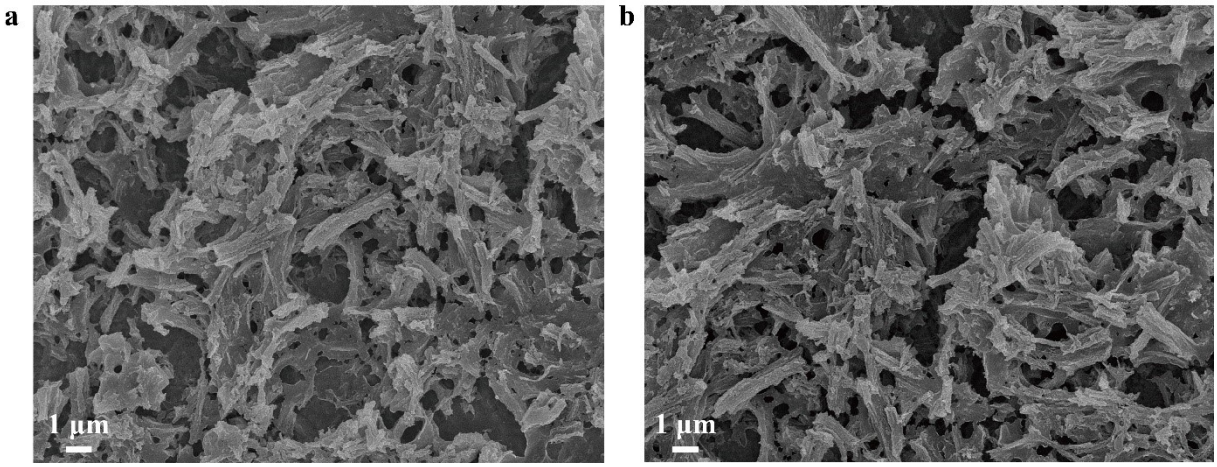

Fig. S18 SEM images of the post-OER P-MoO_2-800.

Fig. S19

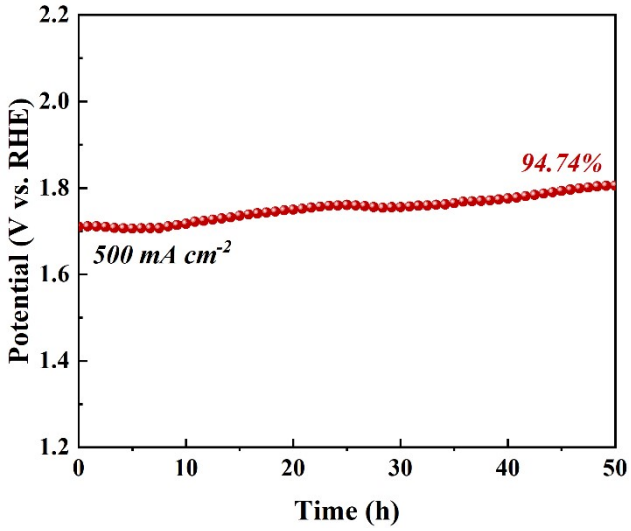

Fig. S19 Stability assessment of P-MoO_2-800 via chronopotentiometry at 500 mA cm^{-2}.

Fig. S20

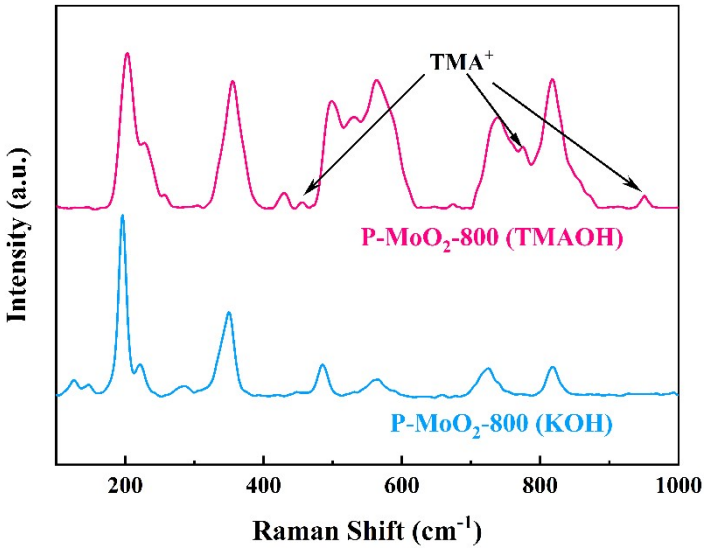

Fig. S20 Raman spectra of P-MoO_2-800 in 1.0 M TMAOH and 1 M KOH after electrolysis.

Fig. S21

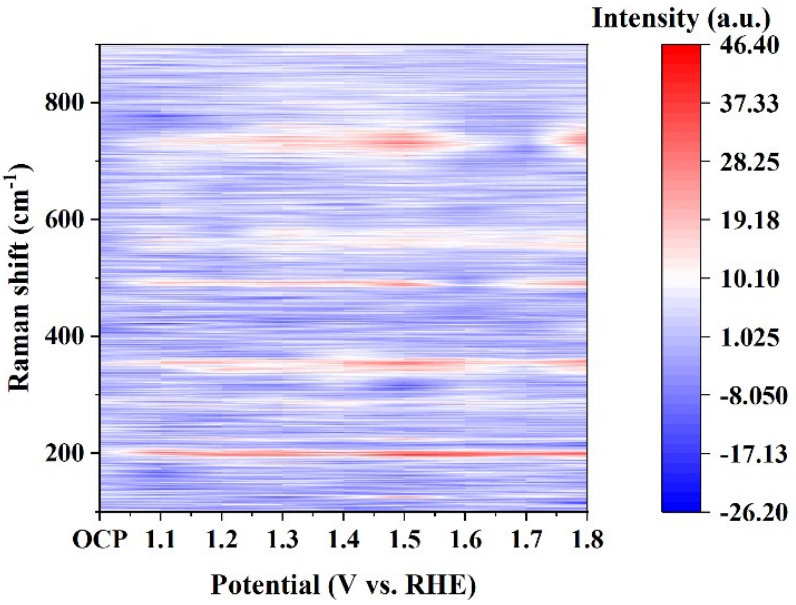

Fig. S21 Contour plot generated from in situ Raman mapping.

Fig. S22

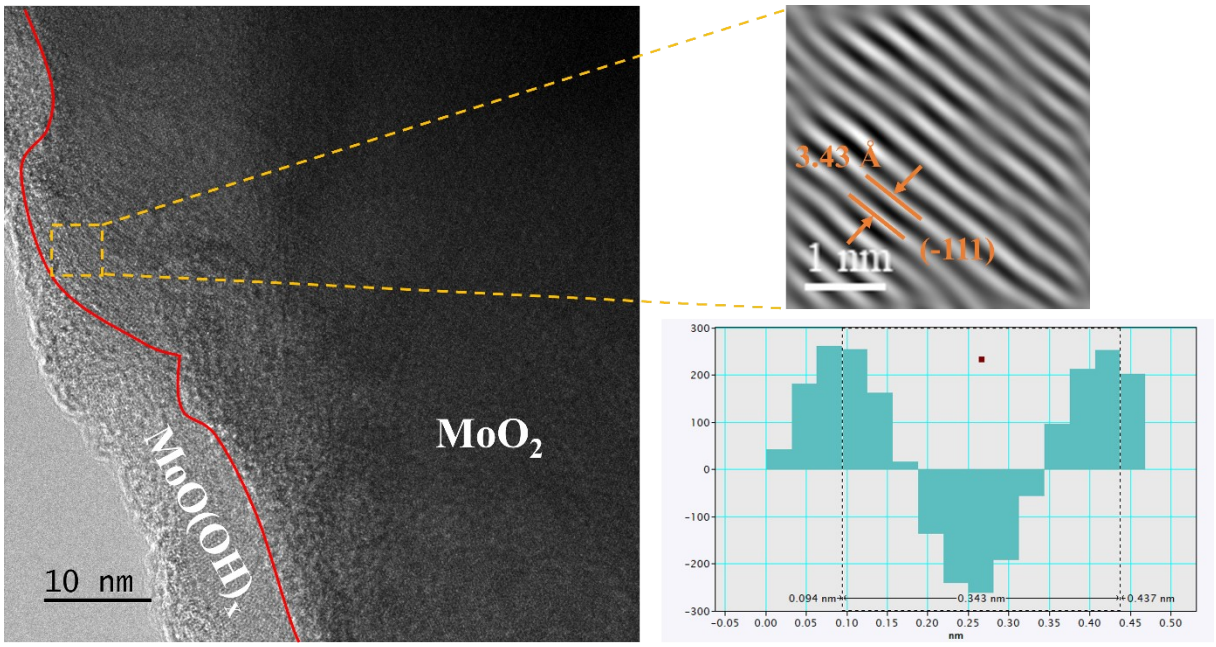

Fig. S22 TEM images of the post-OER P-MoO_2-800.

Fig. S23

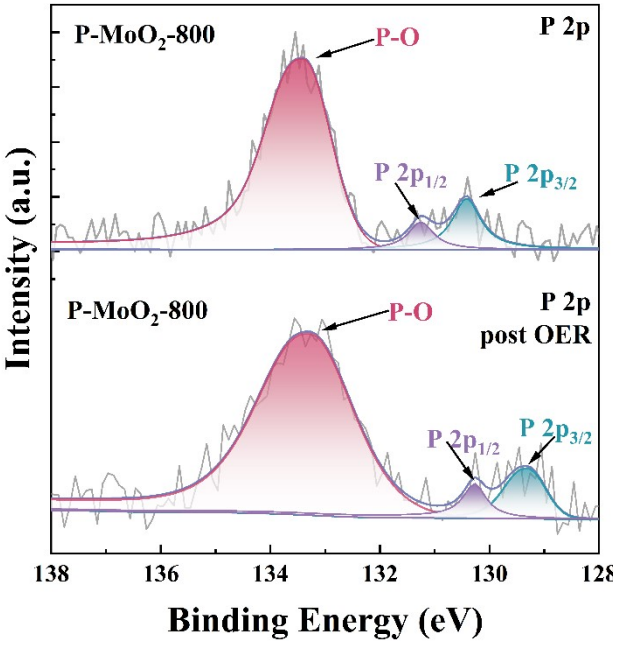

Fig. S23 P 2p XPS spectra before and after the OER.

Fig. S24

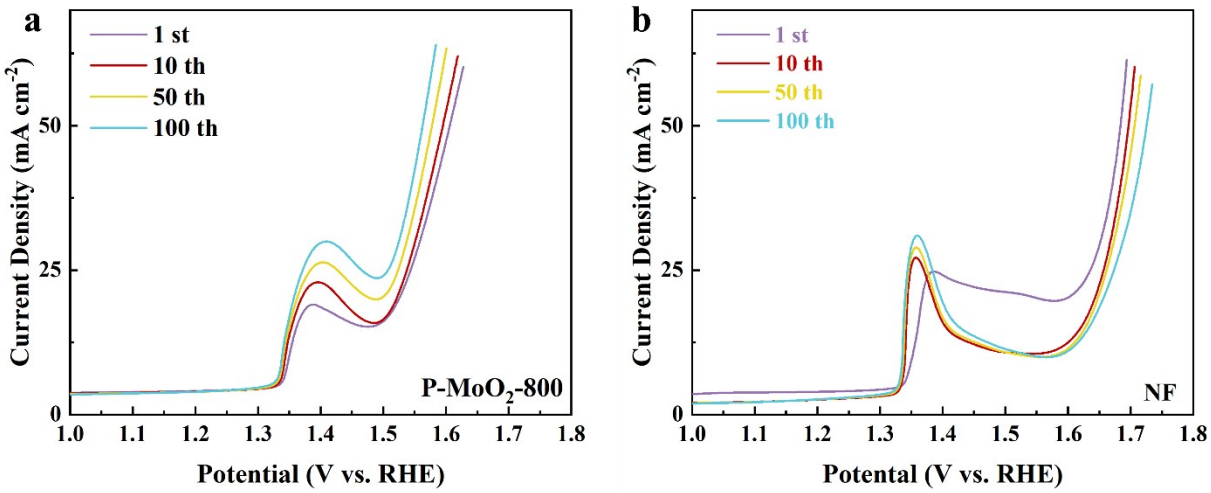

Fig. S24 LSV curves of (a) P-MoO_2-800 and (b) bare NF after different numbers of CV cycles (1st, 10th, 50th, and 100th) in 1.0 M KOH solution.

Table S1. XRD refinement results of MoO_2 and P_{488}–MoO_2-800.

Samples	Lattice parameter α(Å)	Volume V (Å^3)	R_{wp}
MoO_2	5.5488	132.03	10.20
P-MoO_2-800	5.5522	132.10	7.73

Table S2. The ICP-OES analysis data of mass percentage for the samples.

Samples	Mo	P
$P_{0.125}$-MoO_2-800	41.12%	1.18%
$P_{0.25}$-MoO_2-800	40.48%	3.36%
$P_{0.5}$-MoO_2-800	43.07%	5.55%
P_1-MoO_2-800	40.94%	6.67%
P_2-MoO_2-800	40.61%	7.65%
P_4-MoO_2-800	41.83%	8.93%

Table S3. XPS peak-fitting parameters for Mo 3d, O 1s, and P 2p of MoO_2 and P–MoO_2.

Sample	Element	Peak	Binding Energy (eV)	FWHM (eV)	Area (eV)
MoO_2-800	Mo 3d	Mo^{4+}	229.64	0.89	45655.57
		Mo^{4+}	232.69	0.89	31546.33
		Mo^{5+}	231.28	1.92	42696.96
		Mo^{5+}	234.53	1.92	29502.04
		Mo^{6+}	233.20	1.16	26013.74
		Mo^{6+}	236.25	1.16	17594.30
	O 1s	Lattice oxygen	530.46	1.07	75690.97
		Oxygen Vacancy	531.53	1.72	29754.83
		Absorbed water	532.39	1.82	8237.08
P-MoO_2-800	Mo 3d	Mo^{4+}	229.81	0.86	48178.68
		Mo^{4+}	232.99	0.86	33289.71
		Mo^{5+}	231.47	2.26	60838.99
		Mo^{5+}	234.72	2.26	42037.48
		Mo^{6+}	233.52	1.64	28765.44
		Mo^{6+}	236.57	1.64	19361.62
	O 1s	Lattice oxygen	530.5	1.12	55065.13
		Oxygen Vacancy	531.67	2.01	100310.98
		Absorbed water	532.95	1.57	28175.93
	P 2p	$2p_{3/2}$	129.39	0.87	612.76
		$2p_{1/2}$	130.55	0.79	308.73
		P-O	133.56	1.63	4468.06

Table S4. EXAFS fitting parameters at the Mo K-edge of Mo foil, MoO_2, and P-MoO_2-800.

Sample	Shell	*CN* [a]	*R* (Å) [b]	σ^2 ($\times10^{-3}$ Å^2) [c]	ΔE_0 (eV) [d]	*R* factor [e]
Mo foil	Mo-Mo1	8	2.70±0.01	0.0029	7.332	0.0033
	Mo-Mo2	6	3.16±0.01	0.0021		
MoO_2	Mo-O	6	1.96±0.01	0.0043	5.919	0.0121
	Mo-Mo1	2	3.25±0.02	0.0154		
	Mo-Mo2	6	3.69±0.02	0.0055		
P-MoO_2-800	Mo-O	5.283	2.03±0.01	0.0031	5.965	0.0140
	Mo-P	1.032	2.54±0.01	0.0030		
	Mo-Mo1	2.274	2.29±0.03	0.0075		
	Mo-Mo2	6.073	3.72±0.02	0.0060		

Table S5. Comparison of the overpotential and Tafel slope of recently reported transition metal oxides and molybdenum-based electrocatalysts at the current densities of 10 mA cm^{-2} in alkaline solution.

Samples	Overpotential @10 mA cm^{-2} (mV)	Tafel slope (mV/dec)
This work	247	58.04
Ni-Fe-Mo[1]	306	77.1
NiMo-Fe[2]	217	54.28
NiMo-NS[3]	260	54.7
Ni-MoO_2[4]	240	75
Co_3O_4/Fe_2O_3[5]	254	33
Fe-Co-O/Co [6]	257	41.56
CoO/Cu_2O[7]	359	158
Te-$NiFe_2O_4$ [8]	220	44.5
P-$CuCo_2O_4$[9]	250	27
$CoSnO_3$/MXene[10]	274	52
CoFe-P[11]	287	43.2
Ir-NFO[12]	251	30.64
Er-MoO_2 [13]	263	103
$Mo_{0.9}Ni_{0.1}O_2$ [14]	290	90.16
CoP/MoO_2 [15]	282	36.2

References

1. Y. Huang, Y. Wu, Z. Zhang, L. Yang and Q. Zang, *Electrochim. Acta*, 2021, **390**, 138754.
2. H. Liao, X. Zhang, S. Niu, P. Tan, K. Chen, Y. Liu, G. Wang, M. Liu and J. Pan, *Appl. Catal., B*, 2022, **307**, 121150.
3. Y. Liu, P. Liu, Y.-L. Men, Y. Li, C. Peng, S. Xi and Y.-X. Pan, *ACS Appl. Mater. Interfaces*, 2021, **13**, 26064-26073.
4. G. Qian, J. Chen, L. Luo, T. Yu, Y. Wang, W. Jiang, Q. Xu, S. Feng and S. Yin, *ACS Sustainable Chem. Eng.*, 2020, **8**, 12063-12071.
5. Y. Yang, C. Zhu, Y. Zhang, Y. Xie, L. Lv, W. Chen, Y. He and Z. Hu, *J. Phys. Chem. Solids*, 2021, **148**, 109680.
6. T. I. Singh, G. Rajeshkhanna, U. N. Pan, T. Kshetri, H. Lin, N. H. Kim and J. H. Lee, *Small*, 2021, **17**, 2101312.
7. Y. Oh, J. Theerthagiri, M. L. Aruna Kumari, A. Min, C. J. Moon and M. Y. Choi, *J. Energy Chem.*, 2024, **91**, 145-154.
8. Y. Li, H. Guo, J. Zhao, Y. Zhang, L. Zhao and R. Song, *Chem. Eng. J.*, 2023, **464**, 142604.
9. Q. Dong, B. Wen, X. Zhao, P. Wang and X. Lyu, *Sep. Purif. Technol.*, 2025, **353**, 128552.
10. S. Ullah, W. Ahmed, M. Zeeshan, S. Hu and X. Zhang, *Int. J. Hydrogen Energy*, 2024, **70**, 448-460.
11. D. Duan, D. Guo, J. Gao, S. Liu and Y. Wang, *J. Colloid Interface Sci.*, 2022, **622**, 250-260.

12.S. Hong, K. Ham, J. Hwang, S. Kang, M. H. Seo, Y.-W. Choi, B. Han, J. Lee and K. Cho, *Adv. Funct. Mater.*, 2023, **33**, 2209543.
13.T. Yang, H. Lv, Q. Quan, X. Li, H. Lu, X. Cui, G. Liu and L. Jiang, *Appl. Surf. Sci.*, 2023, **615**, 156360.
14.H. He, H. Chen, J. Chen, C. Jia, J. Chen, J. Liang, X. Yao, L. Qin, Y. Huang, D. Chen and Z. Wen, *Chem. Eng. J.*, 2022, **443**, 136339.
15.Z. Liu, Z. Lu, Y. Cao, J. Xie, J. Hu and A. Hao, *Inorg. Chem.*, 2024, **63**, 2803-2813.